JOURNAL OF VIROLOGY, Dec. 1998, p. 10108–10117 Vol. 72, No. 12
0022-538X/98/$04.00+0

CCR5- and CXCR4-Utilizing Strains of Human Immunodeficiency Virus Type 1 Exhibit Differential Tropism and Pathogenesis In Vivo

ROBERT D. BERKOWITZ,[1] SABINA ALEXANDER,[1] CRIS BARE,[1] VALERIE LINQUIST-STEPPS,[1] MARK BOGAN,[1] MARY E. MORENO,[1] LISA GIBSON,[1] ERIC D. WIEDER,[1] JON KOSEK,[2] CHERYL A. STODDART,[1] AND JOSEPH M. MCCUNE[1,3]*

Gladstone Institute of Virology and Immunology[1] and Departments of Microbiology & Immunology and Medicine, University of California, San Francisco,[3] San Francisco, and Department of Pathology, Stanford University, Stanford, and Veterans Hospital, Palo Alto,[2] California

Received 25 June 1998/Accepted 26 August 1998

CCR5-utilizing (R5) and CXCR4-utilizing (X4) strains of human immunodeficiency virus type 1 (HIV-1) have been studied intensively in vitro, but the pathologic correlates of such differential tropism in vivo remain incompletely defined. In this study, X4 and R5 strains of HIV-1 were compared for tropism and pathogenesis in SCID-hu Thy/Liv mice, an in vivo model of human thymopoiesis. The X4 strain NL4-3 replicates quickly and extensively in thymocytes in the cortex and medulla, causing significant depletion. In contrast, the R5 strain Ba-L initially infects stromal cells including macrophages in the thymic medulla, without any obvious pathologic consequence. After a period of 3 to 4 weeks, Ba-L infection slowly spreads through the thymocyte populations, occasionally culminating in thymocyte depletion after week 6 of infection. During the entire time of infection, Ba-L did not mutate into variants capable of utilizing CXCR4. Therefore, X4 strains are highly cytopathic after infection of the human thymus. In contrast, infection with R5 strains of HIV-1 can result in a two-phase process in vivo, involving apparently nonpathogenic replication in medullary stromal cells followed by cytopathic replication in thymocytes.

Infection by most strains of human immunodeficiency virus (HIV) requires interactions with both CD4 and a chemokine receptor termed the coreceptor. X4 strains of HIV type 1 (HIV-1) utilize CXCR4 (16), the receptor for the α-chemokine SDF-1α, while R5 strains of HIV-1 utilize CCR5 (8, 13, 15), a receptor for the β-chemokines MIP-1α, MIP-1β, and RANTES (37). R5 strains have been implicated in horizontal (11, 38, 46) and vertical (2, 34, 39) transmission and are prevalent during the asymptomatic stages of HIV-1 disease (10, 40, 43, 44). X4 strains transmit very poorly and are rarely detected during the asymptomatic stages of HIV-1 disease, but they become prevalent during the symptomatic stages of HIV-1 disease in approximately 50% of individuals (9, 10, 36, 40, 43, 44).

Because X4 strains of HIV-1 are correlated with a decline in peripheral $CD4^+$ T-cell levels and the onset of clinical symptoms (36), they have been considered more pathogenic than R5 strains of HIV-1. Such differential pathogenicity may be related to differences in chemokine receptor expression and, hence, target cell pool size in vivo. Thus, CCR5 is expressed on 5 to 25% of peripheral T cells, mostly $CD4^-$ $CD45RA^-$ memory/effector cells (4, 5, 45), while CXCR4 is expressed on nearly all peripheral T cells (4, 31). Monocytes, the other peripheral blood cell types infected by HIV-1, express CXCR4 (14, 30, 32) but do not appear to be infectable by X4 strains of HIV-1, perhaps due to a postentry block (14). Monocyte differentiation to macrophages in vitro results in CXCR4 downregulation and CCR5 upregulation (14, 32), allowing entry of R5 strains of HIV-1 (17, 24). Wu et al. also observed CCR5 on macrophage-like cells in sections of human lymph nodes (45).

* Corresponding author. Mailing address: Gladstone Institute of Virology and Immunology, P.O. Box 419100, San Francisco, CA 94141-9100. Phone: (415) 695-3828. Fax: (415) 826-8449. E-mail: mike_mccune.givi@quickmail.ucsf.edu.

In addition to being more pathogenic in the periphery, X4 strains may be more effective than R5 strains in decreasing the output of new T cells by the thymus. Autopsy and radiographic studies indicate that the thymus is involuted in patients in later stages of HIV-1 disease (7, 26, 27). Injection of X4 strains of HIV-1 (such as NL4-3) into the human thymus implant in SCID-hu Thy/Liv mice results in the rapid and extensive spread of the virus through all of the $CD4^+$ thymocyte subpopulations: immature $CD4^+$ $CD8^-$ $CD3^-$, intermediate $CD4^+$ $CD8^+$ $CD3^{-/+}$, and mature $CD4^+$ $CD8^-$ $CD3^+$ (3, 20, 41, 42). Concurrent with viral spread, the implants are rapidly depleted of $CD4^+$ thymocytes (3, 6, 18–21, 41, 42) in an apoptotic process which may involve direct and indirect viral effects (3, 6, 19, 42).

Unlike X4 strains, R5 strains of HIV-1 have not been well characterized with regard to thymus infection. In SCID-hu Thy/Liv mice, infection with the R5 strain JR-CSF results in viral spread and thymocyte depletion which is slower than that observed with X4 viruses (3, 6, 18, 41). In another study (21), paired isolates of HIV-1 obtained from seropositive subjects at either early or late stages of disease were evaluated in the context of experimental infection of the Thy/Liv implant. Isolates obtained at early stages of disease were macrophage-tropic, non-syncytium inducing (NSI), and R5-like in their characteristics. Those obtained from patients in the later stages of disease were T-cell tropic, syncytium inducing (SI), and X4-like. The former virus strains, like JR-CSF, replicated slowly within the Thy/Liv implant and caused little if any cytopathicity (as observed during an 8-week time frame). In contrast, the latter X4-like strains spread rapidly and were highly cytopathic. In these studies, however, the exact coreceptor preference of the virus isolates was unknown and the pathogenic role of infected thymic macrophages (which may express CCR5) was not evaluated.

Implicit in the above discussion is the possibility that a switch from relatively nonpathogenic R5 strains to more pathogenic X4 strains may herald the onset of more rapid disease progression in vivo. Such a switch may occur upon selection of a preexisting X4 variant from a dominant population of R5 variants and/or by mutation of an R5-utilizing strain such that it preferentially utilizes CXCR4 instead. Alternatively, R5 strains of HIV-1 may be intrinsically pathogenic but at a slower pace than X4 strains. This possibility is suggested by reports of HIV-1-infected patients who died with T-cell depletion and AIDS and with detectable evidence of NSI strains only (36).

To better characterize the tropism and pathogenesis of R5 strains of HIV-1 in the thymus, we have carried out experimental infections of SCID-hu Thy/Liv implants with the R5 strain Ba-L. We find that Ba-L initially infects medullary stromal cells including macrophages without causing significant pathology. Later, Ba-L enters and slowly spreads through the $CD4^+$ $CD8^+$ thymocyte compartment. In some but not all animals, slow depletion of these cells is also observed. Even after long periods of replication in vivo (e.g., 9 weeks), X4 variants of Ba-L were not detected. These data suggest that R5 viruses can be intrinsically pathogenic in the human thymus.

MATERIALS AND METHODS

Preparation of phytohemagglutinin (PHA)-activated PBMC. Peripheral blood mononuclear cells (PBMC) were isolated from leukocyte-enriched fractions of human blood (Stanford Blood Bank). Equal volumes of cells and phosphate-buffered saline (PBS) containing 10 U of heparin per ml were mixed and underlaid with 15 ml of Histopaque 1077 (Sigma) in 50-ml conical centrifuge tubes and subjected to centrifugation at $450 \times g$ for 30 min. Cells at the interface were collected, washed twice with PBS, counted, and adjusted to 2×10^6 cells per ml in RPMI 1640 medium (Cellgro; Mediatech) containing 10% fetal bovine serum (FBS) and 1 μg of PHA-P (Sigma) per ml. Cells from individual blood donors were incubated separately in 150-cm^2 flasks at 37°C with 5% CO_2 for 3 days, and 10 U of interleukin-2 (IL-2; from human lymphocytes; Boehringer Mannheim, Indianapolis, Ind.) per ml was added the day after cell preparation for the final 2 days of incubation. The cells were then pooled, divided into 1-ml aliquots of 6×10^7 cells per vial in 90% FBS–10% dimethyl sulfoxide (Sigma), and frozen in liquid N_2 for future use.

Preparation of virus. Ba-L (17) stocks were generated in vitro as follows. Human PBMC were cultured in MDM (monocyte-derived macrophage) medium (RPMI 1640, 10% FBS, 5% human AB serum), and nonadherent cells were removed the next day by gentle rinsing with PBS. On day 7, the adherent MDM were infected with a low-passage seed stock of Ba-L virus (NIH AIDS Research and Reference Reagent Program; contributed by Suzanne Gartner, Mikulas Popovic, and Robert Gallo); the medium was collected 8 days later. Fresh medium was added to the culture twice per week during the entire 15-day period.

NL4-3 (1) stocks were generated as follows. Seed virus was prepared by electroporation of 5×10^6 fresh PHA-activated PBMC with 25 μg of NL4-3 plasmid DNA (NIH AIDS Research and Reference Reagent Program; contributed by Malcolm Martin) at 960 μF and 280 V (Bio-Rad Gene Pulser). Working stocks were prepared by inoculating 10^8 fresh PHA-activated PBMC with 2×10^5 50% tissue culture infectious doses ($TCID_{50}$) of virus in 5 ml of IL-2 medium (RPMI 1640 containing 10% FBS and 10 U of IL-2/ml) containing 5 μg of Polybrene (Sigma) per ml. After 2 h at 37°C, the cells were diluted to a density of 2×10^6 to 3×10^6 per ml in IL-2 medium. On day 3 the cells were counted, and an equal number of uninfected PHA-activated PBMC was added for a final concentration of 1.5×10^6 per ml. Virus-containing supernatants were collected daily on days 4 to 7, and fresh cells were added after each collection as described above for day 3.

Each virus-containing supernatant was analyzed for p24 content by enzyme-linked immunosorbent assay (ELISA) (see "p24ELISA" below) and for infectious virus titer by limiting dilution ($TCID_{50}$) assay (see below).

$TCID_{50}$ assay for HIV-1. Thawed PHA-activated PBMC were cultured for 2 days in IL-2 medium and seeded into 96-well plates (10^5 cells in 25 μl per well). Serial half-log dilutions of virus were prepared in medium containing 10 μg of Polybrene per ml, and 25 μl of each dilution was added to quadruplicate wells of PBMC. After 2 h at 37°C, 200 μl of IL-2 medium was added to each well and the plates were incubated at 37°C in a humidified 5% CO_2 atmosphere. After 5 days, the plates were subjected to centrifugation at $400 \times g$ for 5 min and supernatants were assayed for p24 antigen. The $TCID_{50}$ is the reciprocal of the dilution at which 50% of the wells contained detectable p24 (≥30 pg/ml) and specifies the number of infectious doses per 25 μl.

Infection of SCID-hu Thy/Liv mice. All procedures and practices associated with the use of SCID-hu mice were approved by the UCSF Committee on Human Research or the UCSF Committee on Animal Research. SCID-hu Thy/Liv mice were constructed and maintained as described elsewhere (28, 33, 35). Animals within a given cohort were prepared with human fetal tissue from a single donor. Approximately 2,000 $TCID_{50}$ of either virus or an equivalent volume of tissue culture medium (for mock infections) was injected directly into each Thy/Liv implant as described previously (35). After the mice were euthanized by CO_2 asphyxiation and cervical dislocation, the human Thy/Liv implants were removed by surgical excision and placed into either 4% paraformaldehyde (for immunohistochemistry) or 1.5% glutaraldehyde (for electron microscopy) or were transferred to tissue culture dishes containing sterile PBS–2% FBS at 4°C. At times, implants were divided into several pieces for multiple analyses. A single-cell suspension was made by placing the tissue into a sterile nylon bag (Baily Ribbon Mills, Inc.), and while the open end of the bag was closed with a pair of forceps, the tissue was submerged into PBS–2% FBS and gently ground between the nylon layers. The cells were counted on a Coulter counter and used for FACS (fluorescence-activated cell sorting) analysis, cell sorting, p24 ELISA analysis, and coreceptor analysis.

FACS analysis and cell sorting. For analysis of cells from HIV-infected Thy/Liv implants, 10^6 dispersed cells were diluted to 50 μl with monoclonal antibodies (MAbs) CD4-fluorescein isothiocyanate, CD8-phycoerythrin (both from Becton Dickinson Immunocytometry Systems), and CD3-tricolor (Caltag) or with the appropriate isotype control MAbs. For analysis of autofluorescent cells, 10^6 dispersed cells were incubated with CD11c-phycoerythrin and HLA-DR–fluorescein isothiocyanate (Becton Dickinson Immunocytometry Systems) or the appropriate isotype control MAbs. After a 20-min incubation in the dark, the cells were washed with PBS–2% FBS and resuspended in 200 μl of 1% paraformaldehyde. Multiparameter phenotype analysis was carried out on a FACScan (Becton Dickinson Immunocytometry Systems); cell sorting was performed on a FACSVantage (Becton Dickinson Immunocytometry Systems). Thymocytes were sorted for analysis by PCR, while autofluorescent cells were sorted for analysis by PCR, nonspecific esterase (NSE) staining, and assessments of adherence and phagocytosis.

p24 ELISA. One million dispersed cells were collected by brief centrifugation, resuspended in 160 μl of p24 lysis buffer (containing 1% Triton X-100, 0.5% deoxycholate, 5 mM EDTA, 25 mM Tris HCl, 250 mM NaCl, 1% aprotinin), and rotated overnight at 4°C. In the case of virus collections, 10% Triton X-100 was added to a final concentration of 1%. These preparations were then transferred into a quantitative ELISA (DuPont), using HXB2-infected H9 cells to generate a standard curve, as described elsewhere (35).

Immunohistochemistry. Paraformaldehyde-fixed tissue was embedded in paraffin, and 5-μm sections were transferred to glass microscope slides. The sections were deparaffinized by heating to 65°C for 30 min, followed by two 5-min exposures to xylenes. After passage through graded alcohols and rinsing in water, the slides were immersed in 10 mM citric acid (pH 6.0) and microwaved for 10 min. The slides were rinsed in water and exposed to blocking buffer (100 mM Tris HCl, 150 mM NaCl, 0.1% bovine serum albumin) for 20 min at room temperature. The sections were then exposed to purified MAbs specific for either HIV-1 p24 (clone KAL-1; Dako), human CD68 (clone KP1; Dako), or human S100 (clone 15E2E2; Biogenex) in blocking buffer for 1 h at room temperature or overnight at 4°C. After rinsing in Tris-buffered saline (TBS; 100 mM Tris HCl, 150 mM NaCl) for 5 min, the sections were exposed to biotinylated horse anti-mouse immunoglobulin (Vector Laboratories) in blocking buffer containing 4% human AB serum (Sigma) for 30 min at room temperature. The slides were then rinsed in TBS for 5 min and serially exposed to ABC-AP and New Fuchsin detection kits (both from Dako) in the presence of levamisole (Sigma). Finally, the slides were counterstained for 2 min in Mayer's hematoxylin (Sigma), rinsed in water, and mounted with Glycergel (Dako).

For simultaneous detection of two antigens on one section, the sections were first stained for HIV-1 p24 by using the procedure described above through the ABC-AP step. Vector Blue (Vector Laboratories) was used to detect the $p24^+$ cells, after which the slides were immersed in 5 mM EDTA at 80°C for 5 min to inactivate the alkaline phosphatase. The slides were then subjected to a second round of staining for either CD68 or S100, starting with the blocking step and using Vector Red (Vector Laboratories) to detect the positive cells. Counterstaining was not performed.

Electron microscopy. SCID-hu Thy/Liv tissue was fixed for at least 8 h at room temperature in 1.5% glutaraldehyde (cacodylate buffer [pH 7.4]); sucrose was added to bring the milliosmolarity to 300. The tissue was stored at 4°C and dehydrated in ethanol, transferred to propylene oxide, and embedded in Epon 12 resin. Polymerized blocks were sectioned at 0.5 to 1 μm, and the sections were stained with toluidine blue for examination by light microscopy. Selected areas were sectioned at 0.05 μm, enhanced with uranyl acetate and lead citrate, and examined with a Philips 201 electron microscope.

Analysis of sorted autofluorescent cells. Cells that were autofluorescent by flow cytometry were sorted directly onto glass microscope slides, allowed to air dry, and fixed in 2% paraformaldehyde for 10 min at room temperature. After rinsing with water, the slides were assayed for NSE by using an NSE kit with Fast Red (Sigma). For adherence and phagocytosis, autofluorescent cells were sorted directly into eight-chamber slides (Nunc) and cultured overnight with MDM medium. The next day, 1-μm yellow-green carboxylate-modified microspheres (Molecular Probes) were added to the medium for 6 h. The cells were then rinsed gently with PBS, the chamber manifolds were removed, and the slides were mounted with Glycergel (Dako).

PCR. Autofluorescent cells and $CD4^+$ $CD8^+$ thymocytes were sorted into 1.5-ml microcentrifuge tubes and diluted to 100 cells per μl with lysis buffer (100 mM KCl, 10 mM Tris HCl [pH 8.3], 2.5 mM $MgCl_2$, 0.5% Tween 20, 0.5% Nonidet P-40) containing 100 μg of proteinase K per ml (Boehringer Mannheim). The lysates were incubated at 65°C for 30 min, heated to 95°C for 20 min to inactivate the proteinase K, and serially diluted in lysis buffer; 10 μl of each diluted lysate was subjected to HIV-1 *gag* PCR in a 100-μl volume as previously described (29). Fifty microliters of each reaction mixture was subjected to electrophoresis on a 2.5% agarose gel, and reaction products were stained with ethidium bromide.

Coreceptor analysis. HOS cell lines expressing CD4, HIV-1 *tat*-inducible green fluorescent protein (GFP), and either CCR5 or CXCR4 were obtained from the NIH AIDS Research and Reference Reagent Program, contributed by Vineet N. KewalRamani and Dan R. Littman. The cells were cultured in Dulbecco modified Eagle medium containing 10% FBS, 500 μg of G418 per ml, 100 μg of hygromycin per ml, and 1 μg of puromycin per ml; 10^4 cells were seeded into 24-well tissue culture dishes overnight and exposed to virus-containing supernatants or cocultured with dispersed SCID-hu Thy/Liv cells the following day. For NL4-3 and Ba-L virus, 3,000 $TCID_{50}$ was added to the medium and incubated for 6 days. For coculture, 2×10^5 dispersed SCID-hu Thy/Liv cells were suspended in Dulbecco modified Eagle medium containing 10% FBS and added to the indicator cells for 4 to 6 days. Afterwards, the indicator cells were rinsed with PBS, incubated with 300 μl of 1 mM EDTA in PBS for 30 min at room temperature, and removed from the tissue culture dish by gentle pipetting. The suspension was added to 200 μl of 4% paraformaldehyde for 1 h at 4°C and then briefly centrifuged. The supernatant was aspirated, and the cell pellet was suspended in 200 μl of PBS–2% FBS before analysis on a FACScan (Becton Dickinson Immunocytometry Systems).

We also cocultivated 3×10^6 dispersed SCID-hu Thy/Liv cells with 3×10^6 PHA-activated PBMC (see above) to generate high-titer virus for analysis on the coreceptor indicator cell lines. The cell mixture was cultured in 3 ml of IL-2 medium (see above) for 7 to 8 days, after which the cells were removed by brief centrifugation and the supernatant was divided into aliquots and stored at −80°C. After $TCID_{50}$ analysis to determine the titer of the viruses, either 10^3 or 10^4 $TCID_{50}$ was analyzed on the indicator cell lines as described above.

RESULTS

Pathogenesis of R5 and X4 HIV-1 in the Thy/Liv implant. To fully characterize the in vivo phenotype of CCR5-utilizing and CXCR4-utilizing strains of HIV-1, we infected six cohorts of SCID-hu Thy/Liv mice with either the R5 strain Ba-L or the X4 strain NL4-3. The infected implants were harvested at multiple time points thereafter (Tables 1 and 2). Cells were dispersed and analyzed by multiparameter flow cytometry to determine the scatter profiles and the ratios of thymocyte subpopulations. Mock-infected implants contained a small percentage of dead and dying cells (i.e., high-side scatter, low-forward scatter cells lying outside the live-cell scatter gate); among those that were viable, 80 to 90% were usually $CD4^+$ $CD8^+$ thymocytes. The ratio of $CD4^+$ $CD8^-$ thymocytes to $CD4^-$ $CD8^+$ thymocytes was typically between 1.5 and 3. As previously reported, implants infected with NL4-3 were rapidly depleted (Table 1; Fig. 1): the percentage of dead and dying cells increased, the percentage of $CD4^+$ $CD8^+$ thymocytes decreased, and the ratio of $CD4^+$ $CD8^-$thymocytes to $CD8^+$ $CD4^-$ thymocytes inverted. The timing of thymocyte depletion was similar to that seen in previous studies (20, 29, 35): 5 of the 7 implants harvested in the first 2 weeks of infection were not depleted, while all of the 13 implants harvested after week 2 of infection exhibited significant depletion (i.e., the percentage of $CD4^+$ $CD8^+$ thymocytes was less than 60%).

In contrast, infection of SCID-hu Thy/Liv implants with Ba-L resulted in variable degrees of pathology and then only at much later time points. Table 2 summarizes results of experiments using 41 mice prepared from six different donors of human fetal tissue. Within 6 weeks postinoculation, signs of infection (e.g., HIV-1 p24 as measured by ELISA) were evident in 25 of 27 animals (see below). However, depletion of $CD4^+$ $CD8^+$ thymocytes and inversion of the CD4/CD8 ratio was noted in only one of these animals (cohort 1, mouse 17). In the remainder, the profile of thymocyte subpopulations was essentially indistinguishable from that of mock-infected control animals (Fig. 1). Interestingly, $CD4^+$ $CD8^+$ thymocyte depletion was noted in some (5 of 13) animals after week 6 (Table 2, boldface values). Such depletion usually (but not always; see data for cohort 6, mouse 4) was associated with increased levels of viral replication.

TABLE 1. NL4-3 in SCID-hu Thy/Liv mice

Cohort	Day postinoculation	Mouse no.	% Live[a]	% DP[b]	CD4/CD8[c]	p24 (pg/10^6 cells)
2	14	15	63	83	1.3	373
		16	40	70	1.7	909
		17	71	75	2.4	303
	43	18	5	20	0.2	1,474
		19	14	3	0.06	1,565
		20	5	7	0.01	576
3	24	7	29	5	0.6	2,795
		8	26	4	0.7	2,217
		9	21	9	0.7	2,262
		10	4	1	0.4	2,351
4	21	3	42	31	1.3	2,256
5	14	14	37	37	0.7	ND[d]
		15	30	37	0.5	ND
	21	12	21	15	0.2	4,416
		13	55	13	0.6	3,664
		16	39	6	0.4	1,148
6	12	29	83	81	2.3	429
		31	84	84	2.5	42
	26	32	48	24	0.5	1,565
		33	41	9	0.5	1,502

[a] Percentage of events acquired on the FACScan that fall within the live-cell gate.
[b] Percentage of live cells that express CD4 and CD8 (i.e., are double positive [DP]).
[c] Ratio of percentages of $CD4^+$ $CD8^-$ and $CD4^-$ $CD8^+$ thymocytes.
[d] ND, not determined.

Replication of R5 and X4 HIV-1 in the Thy/Liv implant. The relationship between thymocyte depletion and HIV-1 replication in the SCID-hu Thy/Liv implants was assessed by two methods. First, dispersed Thy/Liv cells were lysed and analyzed for intracellular p24 protein by ELISA. p24 protein was detected in all of the Ba-L-infected implants except two implants in cohort 6 which were harvested at day 12 (Table 2). The nondepleted implants exhibited a mean of 57 pg of p24 per million cells in the first 19 days of infection (10 implants) and a mean of 253 pg of p24 per million cells after day 19 (24 implants) (Table 2). The six Ba-L-infected implants with significant depletion exhibited a mean of 719 pg of p24 per million cells. The five nondepleted implants infected with NL4-3 exhibited a mean of 411 pg of p24 per million cells in the first 2 weeks of infection; thereafter, a mean of 1,515 pg per million cells was observed in 13 depleted implants (Table 1). Thus, the pace and extent of thymocyte depletion generally paralleled the degree of viral replication, and by both measures, the kinetics for Ba-L were slower.

Thy/Liv implants infected with Ba-L or NL4-3 were also analyzed for p24 protein by paraffin immunohistochemistry and for virus particles by electron microscopy. Prior to thymocyte depletion, NL4-3-infected implants contained many small, round cells with p24 antigen, likely to be thymocytes, in the thymic cortex (Fig. 2A and B). In contrast, p24-expressing cells in Ba-L-infected implants were large, irregularly shaped, and located primarily in the thymic medulla; these are likely to be

TABLE 2. Ba-L in SCID-hu Thy/Liv mice[a]

Cohort	Day postinoculation	Mouse no.	% Live	% DP	CD4/CD8	p24 (pg/10^6 cells)
1	19	12	85	86	1.5	32
		13	80	80	1.9	32
		14	82	78	1.5	154
		15	80	78	1.2	119
	33	**17**	**59**	**28**	**1.7**	**272**
		18	60	78	1.6	120
		19	73	79	1.3	245
		20	74	74	1.1	115
	48	27	88	79	1.6	272
		28	92	85	0.9	219
		30	**67**	**43**	**0.9**	**1,693**
2	14	25	69	81	2.5	39
		26	72	86	1.7	70
		27	61	89	1.4	44
		28	87	86	2.2	77
	43	**32**	**59**	**59**	**1.7**	**1,191**
		33	**18**	**6**	**1.3**	**540**
		34	63	81	1.2	399
		35	54	85	1.0	836
3	24	25	87	84	1.4	177
		26	88	87	1.8	70
		27	76	89	1.4	79
		28	77	87	2.3	52
4	21	4	64	84	3.3	160
5	14	17	64	79	2.2	ND
	21	19	34	70	1.5	245
		20	83	89	1.3	256
		21	77	90	1.0	490
6	12	1	81	87	2.3	0
		5	82	86	2.5	0
	26	9	68	65	2.5	84
		10	80	84	2.6	21
	35	6	87	76	ND	37
		7	69	64	1.8	473
		11	80	71	2.2	64
	42	3	86	74	2.5	389
		4	**65**	**44**	**1.5**	**63**
		8	86	79	2.1	152
	66	2	76	64	1.5	843
		12	**68**	**49**	**2.0**	**553**
		14	72	68	2.1	283

[a] Values for thymocyte-depleted mice are in boldface. For other details, see the footnotes to Table 1.

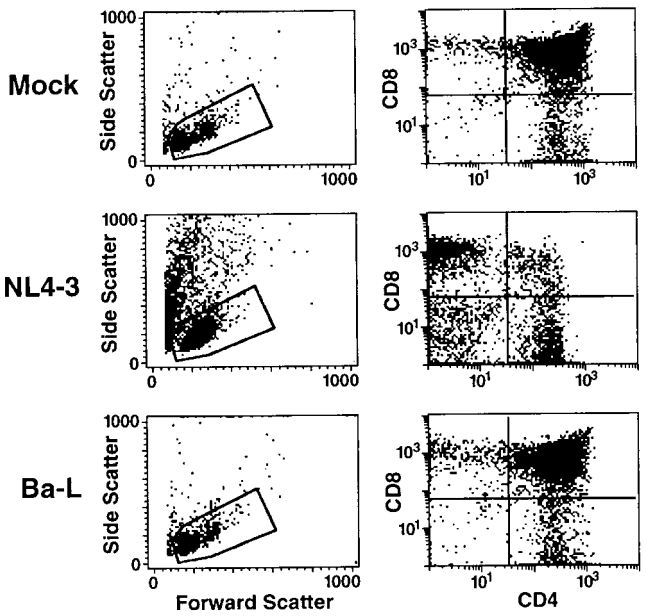

FIG. 1. Pathogenesis of Ba-L and NL4-3 in SCID-hu Thy/Liv mice. Dispersed cells from representative SCID-hu Thy/Liv implants inoculated either with medium (top row), NL4-3 (middle row), or Ba-L (bottom row) were analyzed 21 days postinoculation on a FACScan for forward versus side light scatter properties (left). Events falling within the gate corresponding to live cells were subsequently analyzed for expression of CD4 and CD8 (right).

nonlymphoid stromal cells (Fig. 2C and D). After the third week of infection with Ba-L (Fig. 2E and F), p24 stain was observed at a low frequency in small, round cortical cells, presumably $CD4^+$ $CD8^+$ thymocytes. The frequency of p24 staining of these cells increased over time, with highest densities in implants undergoing thymocyte depletion (Fig. 2F), indicating that Ba-L slowly spread to the cortical thymocytes. Physical evidence for extracellular release and spread of virus was visualized by electron microscopy, with virus particles in regions of cellular debris and in spaces between macrophages and thymocytes (Fig. 2G and H for Ba-L; not shown for NL4-3).

Identity of the stromal cells infected with R5 HIV-1. Phenotypic characterization of the Ba-L-infected cells was initially performed in situ, using MAbs specific for macrophages (CD68) and dendritic cells (S100) on sections adjacent to those stained for p24 protein (Fig. 3A and B). In addition, two-color immunohistochemistry was performed for p24 (labeling cells a blue color) and either CD68 or S100 (labeling cells a red color) on individual Thy/Liv sections; infected macrophages or dendritic cells appeared purple (Fig. 3C to F). In both analyses, most of the $p24^+$ cells appeared to be negative for both S100 and CD68. Occasionally, large, multinucleated $CD68^+$ cells were found to be infected with Ba-L (Fig. 3G). Autofluorescent cells were also detected in the thymic medullae and septae, but these were usually small and in most cases did not appear to be infected (Fig. 3H).

The autofluorescent Thy/Liv cells were analyzed in more detail, phenotypically and with respect to Ba-L infection. Flow cytometric analysis indicated that many of these cells had high side scatter (not shown) and that approximately 50% of them expressed both CD11c and HLA-DR, indicative of a myeloid lineage (Fig. 4A). The autofluorescent cells were purified by FACS and analyzed for the presence of the macrophage enzyme NSE; approximately 80% of the cells were NSE^+ (Fig. 4B). In addition, the sorted autofluorescent cells included cells that were capable of phagocytosis and adherence to plastic (Fig. 4C).

To evaluate whether they were Ba-L infected, autofluorescent cells from 12 implants harvested in the first 3 weeks of infection were sort purified, lysed, serially diluted, and subjected to HIV-1 *gag* PCR analysis to determine the frequency of Ba-L provirus (Table 3; Fig. 5A). Proviral DNA was observed within the autofluorescent cells at a frequency of 1 to 25 genomes per 1,000 cells and was associated with $HLA\text{-}DR^+$ but not $HLA\text{-}DR^-$ autofluorescent cells (data not shown). PCR analysis was also performed on sorted thymocyte subpopulations from Ba-L-infected implants, including $CD4^+$ $CD8^+$ thymocytes (Table 3; Fig. 5A). In implants containing low levels of p24 protein (by ELISA) and no detectable $p24^+$ cortical thymocytes (by immunohistochemistry), proviral DNA

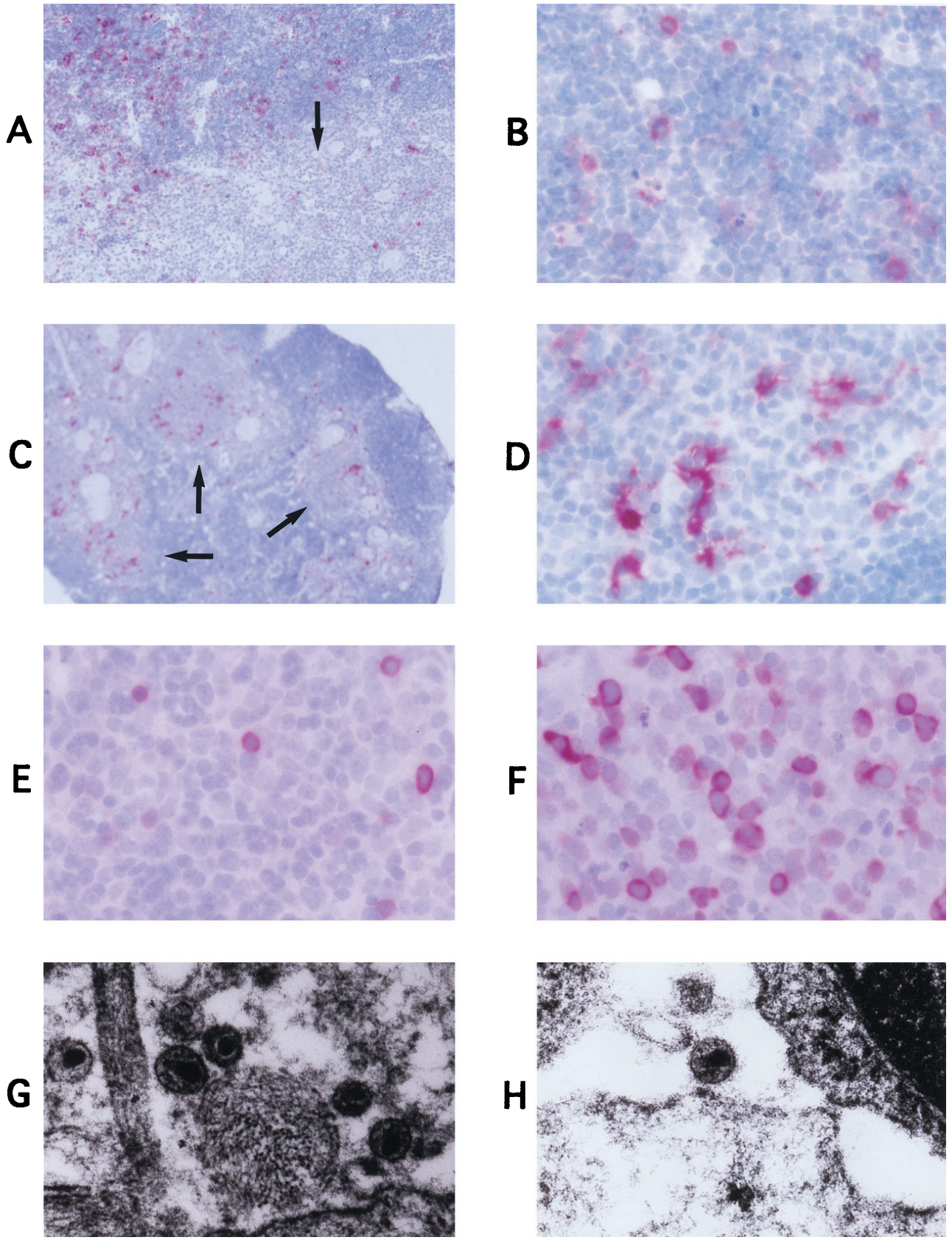

FIG. 2. Tropism of Ba-L and NL4-3 in SCID-hu Thy/Liv mice. (A to F) Immunohistochemical detection of p24 protein (in red) in representative SCID-hu Thy/Liv implants infected either with NL4-3 for 14 days (A and B) or with Ba-L for 14 (C, D), 42 (E), or 66 (F) days. Thymic cortex containing a relatively dense packing of thymocytes can be distinguished from thymic medulla containing a less dense packing of thymocytes (A and C) and Hassell's corpuscles (arrows). An isotype control MAb did not stain any cells, indicating that the p24 signal was antigen specific (data not shown). (G and H) Electron microscopic visualization of Ba-L virus particles in regions of cellular debris (G) or in spaces between whole cells (H; at upper right is a thymocyte). Magnifications: ×4 (C), ×10 (A), ×40 (B and D to F), and ×45,000 (G and H).

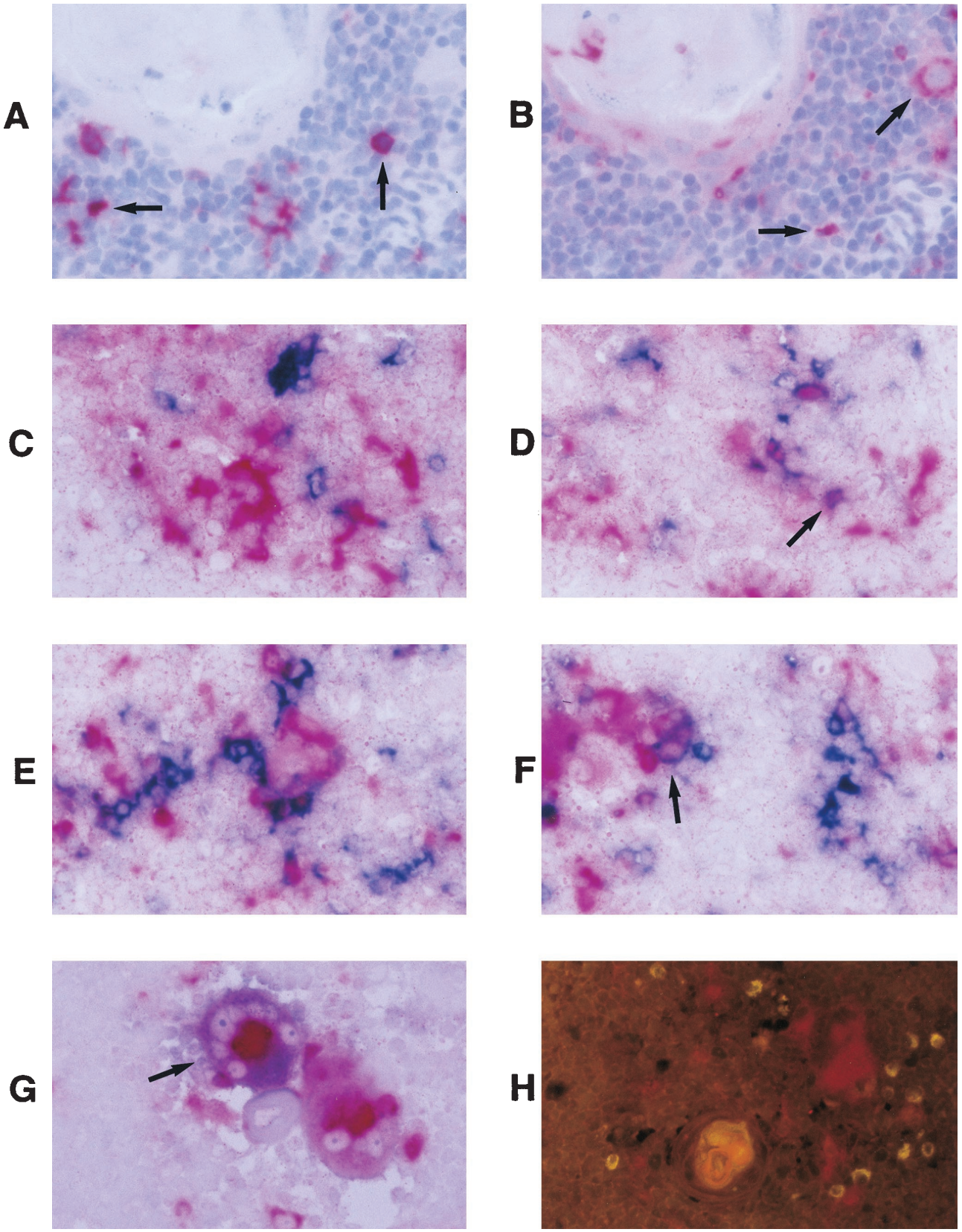

FIG. 3. In situ analysis of the medullary stromal cells infected with Ba-L. (A and B) Immunohistochemical detection of p24 protein (A) or CD68 (B) in serial sections from a representative SCID-hu Thy/Liv implant infected with Ba-L for 14 days. Arrows indicate the position of representative $p24^+$ or $CD68^+$ cells. (C to G) Two-color immunohistochemical detection of p24 protein (blue) and either S100 (C and D) or CD68 (E to G; red) from a representative SCID-hu Thy/Liv implant infected with Ba-L for 33 days. Most cells are either blue or red. Infrequent cells colored purple (and which may be Ba-L-infected dendritic cells or macrophages) are marked with arrows. Panel G depicts two adjacent multinucleated $CD68^+$ medullary macrophages, one infected with Ba-L (purple; arrow) and the other uninfected (red). (H) Dark-field image of a representative Ba-L-infected SCID-hu Thy/Liv implant stained for p24 (red). Autofluorescent cells are apparent (yellow); the large yellow object is a Hassel's corpuscle. Magnification, ×40.

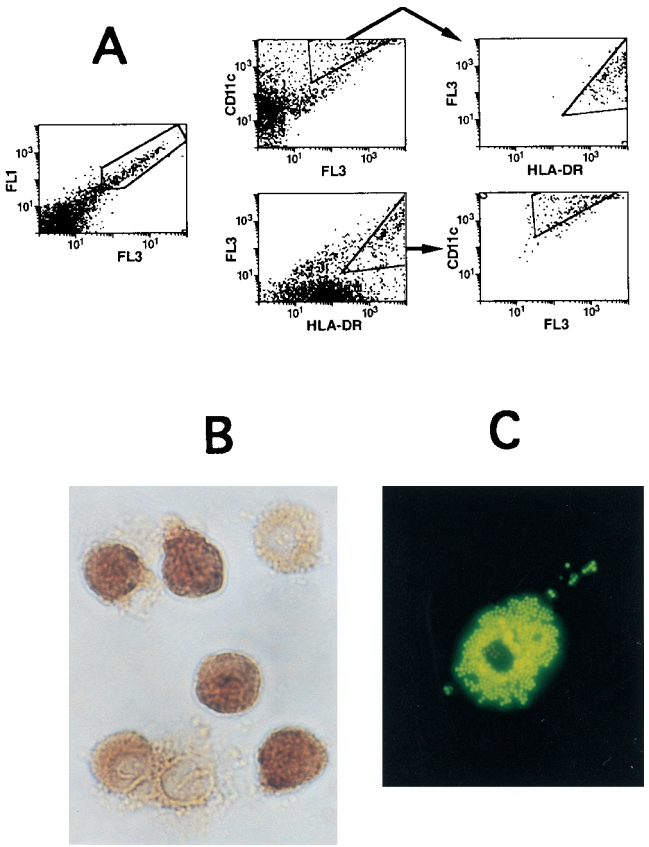

FIG. 4. Analysis of thymic autofluorescent cells. (A) Flow cytometric analysis of CD11c and HLA-DR expression on autofluorescent SCID-hu Thy/Liv cells with high side scatter. (Left) By using mock channels (25), autofluorescent cells are revealed (within gate). (Middle, top row) Cells were analyzed for staining with a CD11c MAb (*y* axis) versus a mock channel (*x* axis). $CD11c^+$ autofluorescent cells were gated and analyzed for HLA-DR expression (right; *x* axis); 95% of $CD11c^+$ cells were $HLA\text{-}DR^+$. (Middle, bottom row) Flow cytometric analysis of the same cells, analyzed for staining with the HLA-DR MAb (*x* axis) versus a mock channel (*y* axis). $HLA\text{-}DR^+$ autofluorescent cells were gated and analyzed for CD11c expression (right; *y* axis); 69% of $HLA\text{-}DR^+$ cells were $CD11c^+$. (B) Sorted autofluorescent cells were stained for NSE (brown color). (C) Sorted autofluorescent cells were cultured overnight, rinsed, and incubated with 1-μm yellow-green microspheres for 6 h. Adherent cells which phagocytosed the microspheres are visible under dark field.

was not detectable in the $CD4^+$ $CD8^+$ thymocytes by PCR. In implants containing intermediate levels of p24 protein (by ELISA) and a low frequency of $p24^+$ cortical thymocytes (by immunohistochemistry; e.g., cohort 5 mice 18, 20, and 21), Ba-L proviral DNA was detected in the $CD4^+$ $CD8^+$ thymocytes at approximately 5 proviruses per 1,000 cells. In contrast, the proviral frequency was higher in sorted cells from five NL4-3-infected implants: 25 to 125 per 1,000 $CD4^+$ $CD8^+$ thymocytes and 5 to 25 per 1,000 autofluorescent cells (Table 3; Fig. 5A).

The relative proviral frequency in sorted thymocytes and autofluorescent cells was calculated (Table 3) and plotted (Fig. 5B) for each Ba-L- or NL4-3-infected implant. For the nine Ba-L-infected implants that contained no detectable proviral DNA in the $CD4^+$ $CD8^+$ thymocytes, a maximum frequency of 1 provirus per 1,000 $CD4^+$ $CD8^+$ thymocytes (the limit of detection in the PCR assay) was assumed. In general, Ba-L infected autofluorescent cells over $CD4^+$ $CD8^+$ thymocytes (with a ratio of 8.67/1), while NL4-3 infected $CD4^+$ $CD8^+$ thymocytes over autofluorescent cells (with a ratio of 1/0.39).

TABLE 3. Detection of Ba-L and NL4-3 proviruses in sorted thymic cells

Cohort	Day post-inoculation	Virus	Mouse no.	No. of proviruses/ 1,000 autofluorescent cells[a]	No. of proviruses/ 1,000 $CD4^+$ $CD8^+$ thymocytes[a]	Ratio[b]
1	19	Ba-L	12	5	<1	>5
			13	5	<1	>5
			14	5	<1	>5
			15	25	<1	>25
2	14	Ba-L	25	5	<1	>5
			26	1	<1	>1
			27	25	<1	>25
			28	1	<1	>1
		NL4-3	15	5	25	0.2
			16	25	100	0.25
5	14	Ba-L	17	25	<1	>25
	21	Ba-L	18	5	5	1
			20	5	5	1
			21	25	5	5
		NL4-3	12	5	25	0.25
			13	25	125	0.25
			16	25	25	1

[a] Calculated from the highest dilution of lysed cells which yields a detectable PCR product (for example, HIV-1 DNA could be detected by PCR in 40 but not 8 autofluorescent cells from mouse 17; thus, 40 cells must contain at least one provirus, and 1,000 cells must contain at least 25 proviruses).

[b] Ratio of the frequency of provirus in autofluorescent cells over the frequency of provirus in $CD4^+$ $CD8^+$ thymocytes.

Coreceptor utilization of Ba-L in vivo. Preferential infection of autofluorescent cells by Ba-L may have been consequent to their expression of CCR5. Yet Ba-L was found to spread to $CD4^+$ $CD8^+$ thymocytes after 3 weeks of infection (Fig. 2 and 5) and to both $CD4^+$ $CD8^+$ thymocytes and $CD3^-$ $CD4^+$ $CD8^-$ intrathymic T progenitor cells after 7 weeks (as determined by PCR analysis of sort-purified cells [data not shown]). Since this latter population has been found to express high levels of CXCR4 and undetectable levels of CCR5 (4), we wondered whether CXCR4-utilizing variants of Ba-L may be responsible for the spread of the virus through thymocytes in the Thy/Liv implants.

To test this possibility, viruses within cohort six Thy/Liv implants harvested 26 to 66 days after infection with Ba-L were assessed for coreceptor utilization (Fig. 6). Total dispersed cells from each of the implants were cocultured with CCR5 and CXCR4 indicator cell lines expressing CD4, either CCR5 or CXCR4, and the HIV-1 *tat*-inducible fluorescent marker GFP (22). Flow cytometric analysis of the indicator cells revealed that for each Ba-L-infected implant, only the CCR5 cell line was infected, even in the implants undergoing thymocyte depletion (Fig. 6). To minimize the possibility that CXCR4-utilizing variants were present but at a frequency too low to be detected in the cocultivation assay, high-titer virus was produced by cocultivating the dispersed thymocytes with PHA-activated PBMC for 7 to 8 days. The indicator cell lines were then infected with 10^4 $TCID_{50}$ of each virus for 5 days; again, for each implant, only the CCR5 cell line was infected (data not shown). These data indicate that CCR5-utilizing, not CXCR4-utilizing, viruses spread through and depleted the thymocytes.

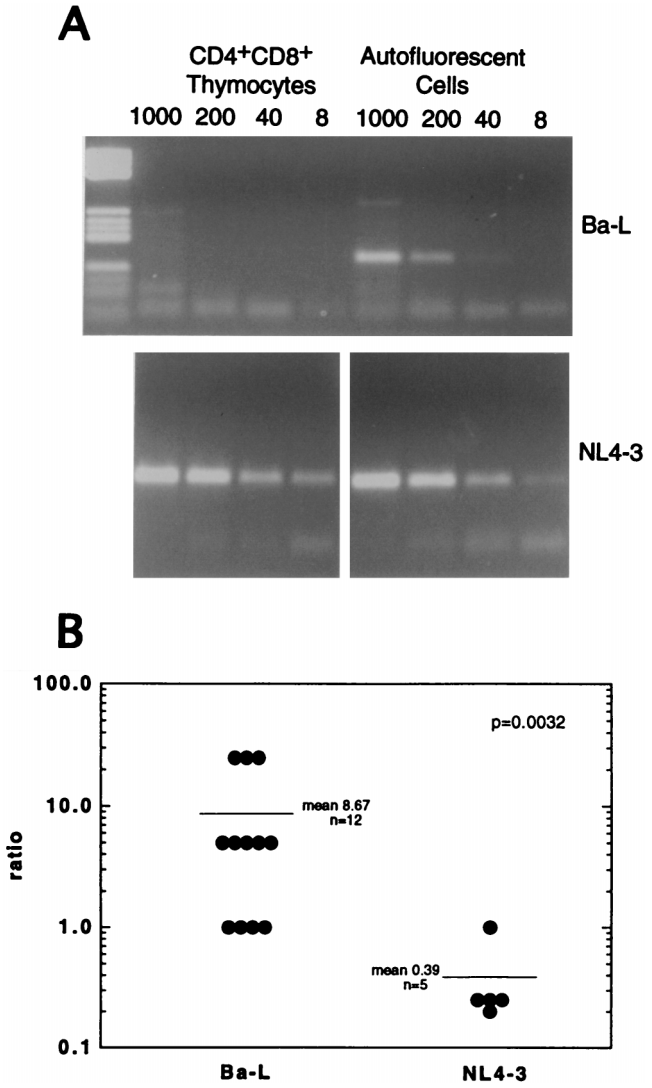

FIG. 5. HIV-1 *gag* PCR analysis of sorted autofluorescent cells and $CD4^+$ $CD8^+$ thymocytes. (A) Autofluorescent cells and $CD4^+$ $CD8^+$ thymocytes from cohort 5 Thy/Liv implants infected with Ba-L (mouse 17) or NL4-3 (mouse 15) were sort purified, lysed, serially diluted, and subjected to PCR using HIV-1 *gag*-specific primers. The PCR products were resolved by agarose gel electrophoresis and stained with ethidium bromide. (B) The ratios of the frequencies of infection of autofluorescent cells and $CD4^+$ $CD8^+$ thymocytes from 17 HIV-1-infected SCID-hu Thy/Liv implants (Table 3) were plotted and analyzed for statistical significance. The mean ratios were 8.67 for Ba-L-infected implants ($n = 12$) and 0.39 for NL4-3-infected implants ($n = 5$), with a Mann-Whitney score of $P = 0.0032$. Note that cohort 5 NL4-3-infected mouse 15 was not included in the statistical analysis because a PCR band was detected in the reaction containing the greatest dilution of input DNA, preventing estimation of the proviral frequency in $CD4^+$ $CD8^+$ thymocytes.

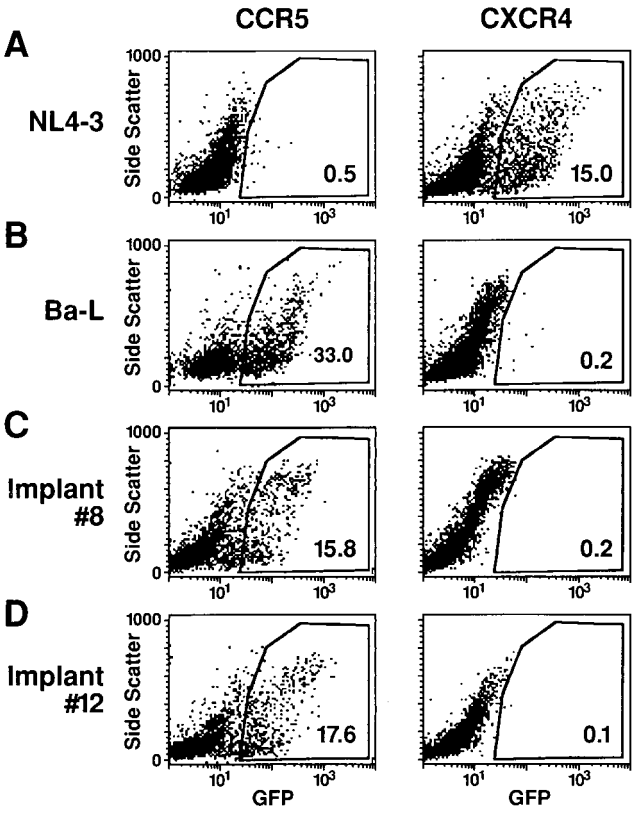

FIG. 6. Coreceptor analysis of virus contained within Ba-L-infected Thy/Liv implants. Indicator cell lines expressing either CCR5 or CXCR4 either were infected with NL4-3 or Ba-L virus or were cultured with dispersed cells from cohort 6 Ba-L-infected Thy/Liv implants 8 and 12, as indicated. After 6 days, the indicator cells were harvested and analyzed by flow cytometry for the expression of HIV-1 *tat*-induced GFP. The percentage of GFP^+ cells is indicated inside each plot.

DISCUSSION

This report provides a detailed description of the tropism and pathogenicity of X4 and R5 HIV-1 strains after infection of the SCID-hu Thy/Liv implant in vivo. As previously reported (20, 35, 42), the X4 strain NL4-3 replicated rapidly in thymocytes and induced thymocyte depletion within 4 weeks in all infected animals. In contrast, the R5 strain Ba-L initially infected stromal cells in the thymic medulla, including cells that have characteristics of macrophages (coexpression of CD11c, HLA-DR, and NSE, adherence to plastic, and phagocytosis). During the first 3 weeks postinfection, there was no discernible evidence of T-cell infection or depletion. During weeks 4 and 5 postinoculation, Ba-L was observed to enter the $CD4^+$ $CD8^+$ thymocyte subpopulation, as detected by PCR and by immunohistochemistry, and thymocytes were depleted in some but not all animals. In such cases, as well as in those wherein no thymocyte depletion was observed, only R5 variants of Ba-L could be rescued from the infected Thy/Liv implant.

These results confirm and extend a previous analysis in which paired NSI and SI isolates of HIV-1 were introduced into SCID-hu Thy/Liv implants (21). The NSI isolates replicated slowly and showed no evidence of T-cell depletion over an 8-week time frame. SI isolates, obtained from the same patients at later stages of disease, were rapidly pathogenic. Given our current results and understanding of HIV-1 tropism, it is likely that the two NSI viruses utilized CCR5 and, like Ba-L, remained preferentially within medullary stromal cells during the 8-week period postinoculation.

Although the inoculum size has varied from study to study, it is apparent from our results and those previously published (3, 6, 18, 21, 41) that R5 viruses can vary in their timing of thymocyte infection and depletion in SCID-hu Thy/Liv implants. Ba-L infection of $CD4^+$ $CD8^+$ thymocytes was detectable only after a delay (3 to 4 weeks in the present study), perhaps due to the fact that CCR5 expression on $CD4^+$ $CD8^+$ thymocytes is relatively low (compared to $CCR5^+$ peripheral T cells [4]). Other primary R5 isolates also exhibit a delay in $CD4^+$ $CD8^+$ thymocyte infection (4a). In contrast, the R5

strain JR-CSF was found (by PCR) in thymocyte subpopulations within the first 3 weeks of inoculation of SCID-hu Thy/Liv mice (3, 18, 41). Like Ba-L, however, JR-CSF was found to spread through the thymocytes more slowly than X4 strains of HIV-1 (18, 41) and to exhibit a delay in thymocyte depletion (6, 18, 41).

Differences in the rates at which X4 and R5 strains spread through and deplete $CD4^+$ $CD8^+$ thymocytes may be due to factors relating to coreceptor utilization. The predominant population of thymocytes ($CD4^+$ $CD8^+$) expresses both CCR5 (4, 12) and CXCR4 (4, 23) and likely serves as the main target for each strain. However, CXCR4 but not CCR5 is expressed at high levels on immature $CD4^+$ $CD8^-$ $CD3^-$ intrathymic T-cell progenitors (ITTPs) (4); injection of the X4 strain NL4-3 into SCID-hu Thy/Liv mice results in the preferential infection of ITTPs over other thymocyte subpopulations (20, 42). Since one ITTP gives rise to hundreds of $CD4^+$ $CD8^+$ thymocytes, proliferation and maturation of X4 virus-infected ITTPs may contribute to the rapid spread of X4 strains through the thymus. Alternatively, infection and destruction of ITTPs by X4 strains of HIV-1 would abrogate thymopoiesis. In either case, thymocyte depletion might occur more rapidly after infection with X4 strains than found in the case of R5 strains.

It is possible that the variable kinetics of infection and thymocyte depletion exhibited by NL4-3 and Ba-L in SCID-hu Thy/Liv implants are due in part to factors other than the viruses' differential coreceptor utilization. For instance, our Ba-L stock was produced in MDM, which might select for virus that replicates inefficiently in thymocytes in vivo. However, this stock was observed to replicate with efficiency similar to that of NL4-3 within PHA-activated PBMCs in vitro. To definitively colocalize the in vivo phenotypes of Ba-L and NL4-3 to differential coreceptor utilization, it will be instructive to directly compare recombinant infectious molecular clones which differ in *env* regions such as V3. These studies are in progress.

The fact that Ba-L could occasionally induce thymocyte depletion without acquiring the ability to utilize CXCR4 suggests that Ba-L is intrinsically pathogenic in the SCID-hu Thy/Liv implant. The mechanisms of pathogenesis are unknown but could include (i) indirect effects mediated by infected stromal cells and cumulative over a long period of time and/or (ii) direct infection and destruction of CCR5-bearing $CD4^+$ $CD8^+$ thymocytes. Additionally, R5 strains like Ba-L may eventually enter and destroy the ITTP subpopulation: although CCR5 was not detectable by flow cytometry on these cells (4), Ba-L proviral DNA was found within them after 7 weeks of infection. Hence, even low levels of expression of CCR5 may be sufficient for viral entry.

In sum, the data presented herein indicate that R5 HIV-1 infects human thymus tissue in two discrete stages: initial infection of medullary stromal cells including macrophages without obvious pathology, followed by slow, pathologic infection of thymocytes. Studies in progress are aimed at understanding the delay in the appearance of the second stage of infection, relative to X4 strains of HIV-1.

ACKNOWLEDGMENTS

This work was supported by grants (to J.M.M.) from the NIH (RO1-AI40312) and from the Elizabeth Glaser Pediatric AIDS Foundation and (to R.D.B.) from the University of California Universitywide AIDS Research Program (R96-GI-041). J.M.M. is an Elizabeth Glaser Scientist supported by the Elizabeth Glaser Pediatric AIDS Foundation.

The following reagents were obtained through the AIDS Research and Reference Reagent Program, Division of AIDS, NIAID, NIH: pNL4-3 from Malcolm Martin; Ba-L from Suzanne Gartner, Mikulas Popovic, and Robert Gallo; and ghost clone 3 CXCR4 and CCR5 cell lines from Vineet N. KewalRamani and Dan R. Littman.

REFERENCES

1. **Adachi, A., H. E. Gendelman, S. Koenig, T. Folks, R. Willey, A. Rabson, and M. A. Martin.** 1986. Production of acquired immunodeficiency syndrome-associated retrovirus in human and nonhuman cells transfected with an infectious molecular clone. J. Virol. **59:**284–291.
2. **Ahmad, N., B. M. Baroudy, R. C. Baker, and C. Chappey.** 1995. Genetic analysis of human immunodeficiency virus type 1 envelope V3 region isolates from mothers and infants after perinatal transmission. J. Virol. **69:**1001–1012.
3. **Aldrovandi, G. M., G. Feuer, L. Gao, B. Jamieson, M. Kristeva, I. S. Chen, and J. A. Zack.** 1993. The SCID-hu mouse as a model for HIV-1 infection. Nature **363:**732–736.
4. **Berkowitz, R. D., K. P. Beckerman, T. J. Schall, and J. M. McCune.** 1998. CXCR4 and CCR5 expression delineates targets for HIV-1 disruption of T cell differentiation. J. Immunol. **161:**3702–3710.

4a. **Berkowitz, R. D., and J. M. McCune.** Unpublished data.

5. **Bleul, C. C., L. Wu, J. A. Hoxie, T. A. Springer, and C. R. Mackay.** 1997. The HIV coreceptors CXCR4 and CCR5 are differentially expressed and regulated on human T lymphocytes. Proc. Natl. Acad. Sci. USA **94:**1925–1930.
6. **Bonyhadi, M. L., L. Rabin, S. Salimi, D. A. Brown, J. Kosek, J. M. McCune, and H. Kaneshima.** 1993. HIV induces thymus depletion *in vivo*. Nature **363:**728–732.
7. **Burke, A. P., D. Anderson, W. Benson, R. Turnicky, P. Mannan, Y. H. Liang, J. Smialek, and R. Virmani.** 1995. Localization of human immunodeficiency virus 1 RNA in thymic tissues from asymptomatic drug addicts. Arch. Pathol. Lab. Med. **119:**36–41.
8. **Choe, H., M. Farzan, Y. Sun, N. Sullivan, B. Rollins, P. D. Ponath, L. Wu, C. R. Mackay, G. LaRosa, W. Newman, N. Gerard, C. Gerard, and J. Sodroski.** 1996. The β-chemokine receptors CCR3 and CCR5 facilitate infection by primary HIV-1 isolates. Cell **85:**1135–1148.
9. **Connor, R. I., and D. D. Ho.** 1994. Human immunodeficiency virus type 1 variants with increased replicative capacity develop during the asymptomatic stage before disease progression. J. Virol. **68:**4400–4408.
10. **Connor, R. I., K. E. Sheridan, D. Ceradini, S. Choe, and N. R. Landau.** 1997. Change in coreceptor use correlates with disease progression in HIV-1-infected individuals. J. Exp. Med. **185:**621–628.
11. **Cornelissen, M., G. Mulder-Kampinga, J. Veenstra, F. Zorgdrager, C. Kuiken, S. Hartman, J. Dekker, L. van der Hoek, C. Sol, R. Coutinho, and J. Goudsmit.** 1995. Syncytium-inducing (SI) phenotype suppression at seroconversion after intramuscular inoculation of a non-syncytium-inducing/SI phenotypically mixed human immunodeficiency virus population. J. Virol. **69:**1810–1818.
12. **Dairaghi, D. J., K. Franz-Bacon, E. Callas, J. Cupp, T. J. Schall, S. A. Tamraz, S. A. Boehme, N. Taylor, and K. B. Bacon.** 1998. Macrophage inflammatory protein-1β induces migration and activation of human thymocytes. Blood **91:**2905–2913.
13. **Deng, H., R. Liu, W. Ellmeier, S. Choe, D. Unutmaz, M. Burkhart, M. P. Di, S. Marmon, R. E. Sutton, C. M. Hill, C. B. Davis, S. C. Peiper, T. J. Schall, D. R. Littman, and N. R. Landau.** 1996. Identification of a major co-receptor for primary isolates of HIV-1. Nature **381:**661–666.
14. **Di Marzio, P., J. Tse, and N. R. Landau.** 1998. Chemokine receptor regulation and HIV type 1 tropism in monocyte-macrophages. AIDS Res. Hum. Retroviruses **14:**129–138.
15. **Dragic, T., V. Litwin, G. P. Allaway, S. R. Martin, Y. Huang, K. A. Nagashima, C. Cayanan, P. J. Maddon, R. A. Koup, J. P. Moore, and W. A. Paxton.** 1996. HIV-1 entry into $CD4^+$ cells is mediated by the chemokine receptor CC-CKR-5. Nature **381:**667–673.
16. **Feng, Y., C. C. Broder, P. E. Kennedy, and E. A. Berger.** 1996. HIV-1 entry cofactor: functional cDNA cloning of a seven-transmembrane, G protein-coupled receptor. Science **272:**872–877.
17. **Gartner, S., P. Markovits, D. M. Markovitz, M. H. Kaplan, R. C. Gallo, and M. Popovic.** 1986. The role of mononuclear phagocytes in HTLV-III/LAV infection. Science **233:**215–219.
18. **Jamieson, B. D., S. Pang, G. M. Aldrovandi, J. Zha, and J. A. Zack.** 1995. In vivo pathogenic properties of two clonal human immunodeficiency virus type 1 isolates. J. Virol. **69:**6259–6264.
19. **Jamieson, B. D., C. H. Uittenbogaart, I. Schmid, and J. A. Zack.** 1997. High viral burden and rapid $CD4^+$ cell depletion in human immunodeficiency virus type 1-infected SCID-hu mice suggest direct viral killing of thymocytes in vivo. J. Virol. **71:**8245–8253.
20. **Jenkins, M., M. B. Hanley, M. B. Moreno, E. Wieder, and J. M. McCune.** 1998. HIV-1 infection interrupts thymopoiesis and multilineage hematopoiesis *in vivo*. Blood **91:**2672–2678.
21. **Kaneshima, H., L. Su, M. L. Bonyhadi, R. I. Connor, D. D. Ho, and J. M. McCune.** 1994. Rapid-high, syncytium-inducing isolates of human immunodeficiency virus type 1 induce cytopathicity in the human thymus of the SCID-hu mouse. J. Virol. **68:**8188–8192.
22. **KewalRamani, V., and D. Littman.** Unpublished data.

23. **Kitchen, S. G., and J. A. Zack.** 1997. CXCR4 expression during lymphopoiesis: implications for human immunodeficiency virus type 1 infection of the thymus. J. Virol. **71:**6928–6934.
24. **Koyanagi, Y., S. Miles, R. T. Mitsuyasu, J. E. Merrill, H. V. Vinters, and I. S. Chen.** 1987. Dual infection of the central nervous system by AIDS viruses with distinct cellular tropisms. Science **236:**819–822.
25. **Liu-Wu, Y., A. Svenningsson, S. Stemme, J. Holm, and O. Wiklund.** 1997. Identification and analysis of macrophage-derived foam cells from human atherosclerotic lesions by using a "mock" FL3 channel in flow cytometry. Cytometry **29:**155–164.
26. **McCune, J. M., and H. Kaneshima.** 1995. The hematopathology of HIV-1 disease: experimental analysis *in vivo*, p. 129–156. *In* M. G. Roncarolo, B. Namikawa, and R. Péault (ed.), Human hematopoiesis in SCID mice. R. G. Landes Company, Austin, Tex.
27. **McCune, J. M., R. Loftus, D. K. Schmidt, P. Carroll, D. Webster, B. Swor-Yim, I. R. Francis, B. H. Gross, and R. M. Grant.** 1998. High prevalence of thymic tissue in adults with HIV-1 infection. J. Clin. Invest. **101:**2301–2308.
28. **McCune, J. M., R. Namikawa, H. Kaneshima, L. D. Shultz, M. Lieberman, and I. L. Weissman.** 1988. The SCID-hu mouse: murine model for the analysis of human hematolymphoid differentiation and function. Science **241:**1632–1639.
29. **McCune, J. M., R. Namikawa, C. C. Shih, L. Rabin, and H. Kaneshima.** 1990. Suppression of HIV infection in AZT-treated SCID-hu mice. Science **247:**564–566.
30. **McKnight, A., D. Wilkinson, G. Simmons, S. Talbot, L. Picard, M. Ahuja, M. Marsh, J. A. Hoxie, and P. R. Clapham.** 1997. Inhibition of human immunodeficiency virus fusion by a monoclonal antibody to a coreceptor (CXCR4) is both cell type and virus strain dependent. J. Virol. **71:**1692–1696.
31. **Mo, H., S. Monard, H. Pollack, J. Ip, G. Rochford, L. Wu, J. Hoxie, W. Borkowsky, D. P. Ho, and J. P. Moore.** 1998. Expression patterns of the HIV type 1 coreceptors CCR5 and CXCR4 on $CD4^+$ T cells and monocytes from cord and adult blood. AIDS Res. Hum. Retroviruses **14:**607–617.
32. **Naif, H. M., S. Li, M. Alali, A. Sloane, L. Wu, M. Kelly, G. Lynch, A. Lloyd, and A. L. Cunningham.** 1998. CCR5 expression correlates with susceptibility of maturing monocytes to human immunodeficiency virus type 1 infection. J. Virol. **72:**830–836.
33. **Namikawa, R., K. N. Weilbaecher, H. Kaneshima, E. J. Yee, and J. M. McCune.** 1990. Long-term human hematopoiesis in the SCID-hu mouse. J. Exp. Med. **172:**1055–1063.
34. **Ometto, L., C. Zanotto, A. Maccabruni, D. Caselli, D. Truscia, C. Giaquinto, E. Ruga, L. Chieco-Bianchi, and A. De Rossi.** 1995. Viral phenotype and host-cell susceptibility to HIV-1 infection as risk factors for mother-to-child HIV-1 transmission. AIDS **9:**427–434.
35. **Rabin, L., M. Hincenbergs, M. B. Moreno, S. Warren, V. Linquist, R. Datema, B. Charpiot, J. Seifert, H. Kaneshima, and J. M. McCune.** 1996. Use of standardized SCID-hu Thy/Liv mouse model for preclinical efficacy testing of anti-human immunodeficiency virus type 1 compounds. Antimicrob. Agents Chemother. **40:**755–762.
36. **Richman, D. D., and S. A. Bozzette.** 1994. The impact of the syncytium-inducing phenotype of human immunodeficiency virus on disease progression. J. Infect. Dis. **169:**968–974.
37. **Rollins, B. J.** 1997. Chemokines. Blood **90:**909–928.
38. **Roos, M. T., J. M. Lange, G. R. de, R. A. Coutinho, P. T. Schellekens, F. Miedema, and M. Tersmette.** 1992. Viral phenotype and immune response in primary human immunodeficiency virus type 1 infection. J. Infect. Dis. **165:**427–432.
39. **Scarlatti, G., V. Hodara, P. Rossi, L. Muggiasca, A. Bucceri, J. Albert, and E. M. Fenyo.** 1993. Transmission of human immunodeficiency virus type 1 (HIV-1) from mother to child correlates with viral phenotype. Virology **197:**624–629.
40. **Schuitemaker, H., M. Koot, N. A. Kootstra, M. W. Dercksen, G. R. de, S. R. van, J. M. Lange, J. K. Schattenkerk, F. Miedema, and M. Tersmette.** 1992. Biological phenotype of human immunodeficiency virus type 1 clones at different stages of infection: progression of disease is associated with a shift from monocytotropic to T-cell-tropic virus population. J. Virol. **66:**1354–1360.
41. **Stanley, S. K., J. M. McCune, H. Kaneshima, J. S. Justement, M. Sullivan, E. Boone, M. Baseler, J. Adelsberger, M. Bonyhadi, J. Orenstein, C. H. Fox, and A. S. Fauci.** 1993. Human immunodeficiency virus infection of the human thymus and disruption of the thymic microenvironment in the SCID-hu mouse. J. Exp. Med. **178:**1151–1163.
42. **Su, L., H. Kaneshima, M. Bonyhadi, S. Salimi, D. Kraft, L. Rabin, and J. M. McCune.** 1995. HIV-1-induced thymocyte depletion is associated with indirect cytopathogenicity and infection of progenitor cells *in vivo*. Immunity **2:**25–36.
43. **Tersmette, M., R. E. de Goede, B. J. Al, I. N. Winkel, R. A. Gruters, H. T. Cuypers, H. G. Huisman, and F. Miedema.** 1988. Differential syncytium-inducing capacity of human immunodeficiency virus isolates: frequent detection of syncytium-inducing isolates in patients with acquired immunodeficiency syndrome (AIDS) and AIDS-related complex. J. Virol. **62:**2026–2032.
44. **Tersmette, M., R. A. Gruters, W. F. de, G. R. de, J. M. Lange, P. T. Schellekens, J. Goudsmit, H. G. Huisman, and F. Miedema.** 1989. Evidence for a role of virulent human immunodeficiency virus (HIV) variants in the pathogenesis of acquired immunodeficiency syndrome: studies on sequential HIV isolates. J. Virol. **63:**2118–2125.
45. **Wu, L., W. A. Paxton, N. Kassam, N. Ruffing, J. B. Rottman, N. Sullivan, H. Choe, J. Sodroski, W. Newman, R. A. Koup, and C. R. Mackay.** 1997. CCR5 levels and expression pattern correlate with infectability by macrophage-tropic HIV-1 *in vitro*. J. Exp. Med. **185:**1681–1691.
46. **Zhu, T., H. Mo, N. Wang, D. S. Nam, Y. Cao, R. A. Koup, and D. D. Ho.** 1993. Genotypic and phenotypic characterization of HIV-1 patients with primary infection. Science **261:**1179–1181.